Effect of Glycerol on the Interactions and Solubility of Bovine Pancreatic Trypsin Inhibitor

Michael Farnum and Charles Zukoski
The Department of Chemical Engineering, University of Illinois at Urbana-Champaign, Urbana, Illinois 61801 USA

ABSTRACT The effects of additives used to stabilize protein structure during crystallization on protein solution phase behavior are poorly understood. Here we investigate the effect of glycerol and ionic strength on the solubility and strength of interactions of the bovine pancreatic trypsin inhibitor. These two variables are found to have opposite effects on the intermolecular forces; attractions increase with [NaCl], whereas repulsions increase with glycerol concentration. These changes are mirrored in bovine pancreatic trypsin inhibitor solubility where the typical salting out behavior for NaCl is observed with higher solubility found in buffers containing glycerol. The increased repulsions induced by glycerol can be explained by a number of possible mechanisms, all of which require small changes in the protein or the solvent in its immediate vicinity. Bovine pancreatic trypsin inhibitor follows the same general phase behavior as other globular macromolecules where a robust correlation between protein solution second virial coefficient and solubility has been developed. This study extends previous reports of this correlation to solution conditions involving nonelectrolyte additives.

INTRODUCTION

Most of the detailed information of the molecular structure of biological molecules has been derived from x-ray crystallography. Considerable advances have been made in methods of protein production and purification as well as in instrumentation and computational methods to analyze the x-ray data (McRee, 1993; Drenth, 1994). As a result of the relative availability of proteins and the relative ease of analysis of scattering data, the bottleneck of protein structure determination is the growth of high quality crystals (McPherson, 1990).

A knowledge of the protein solution phase behavior is crucial for the development of methods to grow high quality crystals. Solubility depends on many factors, including the solvent, temperature, and pressure. The solvents used are often complex aqueous mixtures of buffer salts with organic solvents and surfactants sometimes added as well. How each of these additives alters solubility is largely unexplored. As a result, methods for choosing crystallization conditions are largely empirical and derived from a knowledge of conditions that have worked in the past (McPherson, 1982).

Recently, George and Wilson observed that the osmotic second virial coefficient of protein solutions falls in a narrow range when measured under crystallizing conditions (George and Wilson, 1994; George et al., 1997). The second virial coefficient is a measure of the strength of protein interactions. A positive value indicates that the proteins are repulsive, and a negative value indicates attractions (McQuarrie, 1976). The virial coefficients found by George and Wilson were slightly negative at conditions where high quality crystals were grown. Using this method as a quick diagnostic provides a way to determine if the conditions for selected crystallization are correct without the long waiting period necessary for actual crystal growth.

A quantitative link between the second virial coefficient and the solubility behavior was established by treating the proteins as interacting with simple, centrosymmetric interaction potentials (Rosenbaum et al., 1996). This analysis is based on proteins crystallizing under conditions where they experience attractions that have an extent that is a small fraction of the protein diameter. This analysis also provided insight into origin of the metastable liquid-liquid phase separation observed in many protein solutions under conditions of strong attractions (Rosenbaum and Zukoski, 1996; Fine et al., 1996). These studies suggest that at the same appropriately normalized second virial coefficient, large classes of globular proteins will have the same dimensionless solubility. This observation has been confirmed for a variety of systems where the suspending solvent is composed of a buffer and a strong electrolyte for proteins that are relatively symmetric and have with small dipole moments (Rosenbaum and Zukoski, 1996; Fine et al., 1996).

However, many protein crystallization solvents are complex mixtures containing polymers, polyols, and metal ions (McPherson, 1982). The role of these additives is poorly understood. Polyols, a common ingredient in these crystallization cocktails, have been shown to stabilize protein structure (Sousa, 1995; Gekko and Timasheff, 1981). Polyols contain hydrocarbon chains with multiple hydroxyl groups that allow hydrogen bonding with water and include a number of natural compounds, such as sugars, polysaccharides, and glycerol, as well as synthetic polymers such as polyethylene glycol. How these additives alter the correlation between second virial coefficient and solubility is largely unexplored.

Received for publication12 June 1998 and in final form 27 January 1999.
Address reprint requests to Dr. Charles F. Zukoski, Department of Chemical Engineering, University of Illinois, 114 Roger Adams Lab, Box C-3, 600 S. Mathews Avenue, Urbana, IL 61801. Tel.: 217-244-9214; Fax: 217-333-5052; E-mail: czukoski@uiuc.edu.

0006-3495/99/05/2716/11 $2.00

Glycerol has the property of stabilizing protein structure (Sousa, 1995). As a result, if crystallization occurs over a long period of time, glycerol is a useful candidate to be part of the crystallization solvent and is often included for this purpose. Priev et al. (1996) studied the effect of glycerol on the specific volumes of several proteins, sugars, and amino acids. Their work indicates that the addition of glycerol decreases the volume of the protein core by 8% resulting in a reduction in the radius of an equivalent sphere by only 2.6%: a small distance for most proteins with radii of several nanometers. However, Priev et al. also suggested the addition of glycerol increases hydration at the particle surface. Larger molecules, such as proteins, show a net decrease in volume because they have a large core and internal effects dominate. For the small molecules, such as sugars and amino acids, surface effects dominate, and the specific volume increases. In addition, compression of the protein core may alter the extent to which different amino acids are exposed or buried in the presence of the additive. Thus depending on the protein surface chemistry, size, and flexibility, glycerol may alter the protein in a number of ways. Changes in protein size or surface characteristics can have large effects of protein interactions and thus on solubility. As a consequence, we anticipate that addition of glycerol will alter protein phase diagrams. Here we explore both how glycerol alters interaction strength and solubility and thus provide an additional test of the correlation of Rosenbaum et al. (1996).

Bovine pancreatic trypsin inhibitor (BPTI) was chosen for these studies as it has been characterized by a number of techniques and has served as a model protein for a number of studies (Creighton, 1974; Amir et al., 1992; Lakowicz et al., 1987). BPTI consists of a single chain of 58 amino acids with a molecular weight of 6511 g mol^{-1} containing three disulfide bonds (Kassell, 1970), making it extremely stable at room temperature (Makhatadze et al., 1993). From the crystal structure (1BPI, Brookhaven Databank), the protein is known to be ellipsoidal with a major axis diameter of ~2.9 nm and a minor axis diameter of 1.9 nm with an equivalent diameter of an unhydrated sphere determined from diffusivity measurements of 2.48 nm (Gallagher and Woodward, 1989). The isoelectric point of BPTI is ~10.5 (Wuthrich and Wagner, 1979). Using the pK_a values determined by Wuthrich and Wagner, BPTI carries a charge of approximately +6.2 at pH 4.9 with a dipole moment estimated to be 280 Debye. Whereas there has been some disagreement over its aggregation state at pH 4.9 (Gallagher and Woodward, 1989; Scholtan and Lie, 1966; Lafont et al., 1996, 1997; Wills and Georgalis, 1981), BPTI has been studied as a model protein for crystallization experiments (Lafont et al., 1994).

Below we describe our experimental methods in section II before discussing the effects of glycerol and ionic strength on BPTI second virial coefficients and solubility in section III. These results are discussed in section IV in terms of generalized phase diagrams and conventional colloid interaction potentials. In section V, conclusions are drawn.

EXPERIMENTAL METHODS

Protein interactions were characterized in dilute solutions by static light scattering. For particles small relative to the wavelength of the incident light, the behavior is governed by the Raleigh scattering equation,

$$\lim_{c \leftarrow 0} \frac{Kc}{R_\theta} = \frac{1}{M_w} + \frac{2B_2 N_A}{M_w^2} c \qquad (1)$$

in which K is an optical constant, c is the mass concentration, R_θ is the Rayleigh ratio, M_W is the molecular weight of the protein, B_2 is the second virial coefficient, and N_A is Avogadro's number. B_2 provides an integral measure of protein-protein interactions with positive values indicating repulsions and negative values reflecting attractions. The optical constant K depends on the scattering properties of the chosen system,

$$K = \frac{4\pi^2 [n_s (dn/dc)]^2}{N_A \lambda^4}. \qquad (2)$$

in which λ is wavelength of the incident radiation in the medium, dn/dc is the refractive index increment of the particle in a particular solvent, and n_s is the refractive index of the solvent.

Static-light scattering was performed using a Brookhaven Instruments BI-200SM goniometer. Both a Spectra-Physics 60 mW He-Ne laser at 632.8 nm and a Lexel Laser Argon-Ion Model 95 laser operating at 514 nm were used. The sample cell, which consisted of a glass test tube, was contained in a constant temperature bath of index matching fluid, dodecahydronapthylene. The index matching fluid was filtered through a 0.2-μm filter to remove dust. The temperature of the index-matching fluid was maintained by a recirculating bath fluid, which heated and cooled a plate beneath the decalin bath as necessary. All experiments in this study were carried out at 20°C with data taken at angles between 60° and 120°. Light intensity was measured with a photomultiplier tube with the output signal processed by a BI-9000AT digital correlator.

For each experiment, the apparatus is calibrated with toluene. The Rayleigh ratio of toluene has been determined experimentally to be 14.02×10^6 cm^{-1} at 632.8 nm (Kaye and McDaniel, 1974) and estimated to be 32×10^6 cm^{-1} at 514.5 nm (Coumou, 1960; Coumou et al., 1964; Coumou and Mackor, 1964).

BPTI was purchased from Sigma (Aprotinin, A 1153) and was normally used without further purification. Dry protein powder was dissolved into solvent twice filtered through 0.02-mm Anotop inorganic syringe filters (Altech Associates Inc). The protein stock solutions were then filtered through 0.2-μm cellulose acetate filters at least three times followed by at least five filtrations through 0.02-μm Anotop filters. Before filtration, both static and dynamic light scattering from the solutions indicate the presence of a fraction of significantly larger particles than protein monomers.

Buffer solutions were prepared by dissolving acetic acid and sodium acetate (60 mM) in distilled water, deionized by a Millipore system ($< 10^{-6}$ M) so that the ionic strength was known precisely. Sodium chloride was then added to these buffer solutions. In the case of the glycerol buffer solutions, the distilled water solution was replaced by a glycerol/water mixture of the appropriate weight fraction. The pH of each of the solvent buffers was measured to be within 0.05 pH units of the desired value of 4.9 in all cases before the addition of BPTI.

The concentrations of the filtered BPTI solutions are determined by measuring the absorbance of the solutions at 280 nm, a characteristic protein absorbance. Both a Bausch and Lomb Spectronic 1001 spectrophotometer and a Hewlett Packard 8453 UV-Vis spectrophotometer were used. A calibration curve was made using unfiltered protein solutions, which gave an extinction coefficient of 0.692 ± 0.008 ml/mg cm at 280 nm. The absorbance from the protein solutions did not change by a measurable amount, indicating that a negligible amount of protein was lost and that the large impurities were not protein aggregates. Because the calibration curve was linear with BPTI concentrations less than 3.5 mg/ml, following a typical Beer's law behavior, all spectrophotometric measurements were made after diluting the protein solutions to this range.

The radius of a BPTI monomer calculated from thermal denaturation experiments (Makhatadze et al., 1993) is 1.22 ± 0.01 nm, which agrees well with crystallographic results (Parkin et al., 1996; Deisenhofer and Steigemann, 1975). As expected, the scattering data indicate that there is no angular dependence in the measured Rayleigh ratios. Demonstrating a lack of angular dependence of R_θ gives clear evidence of the absence of any significant fraction of large particles in solution (Kerker, 1969). In a few cases, there was a strong angular dependence of the Rayleigh ratio on the angle and for these samples dynamic light scattering results showed the presence of particles approximately with a 100-nm radius. Upon filtration, these impurities were removed, and no aggregates reformed in these solutions.

In order to determine an absolute measure of the molecular weight, the refractive index increment, *dn*/*dc*, of the particle in the solvent must be known. The value used was 0.186 ml/g (Gallagher and Woodward, 1989), which was measured for BPTI in a variety of aqueous NaCl solutions with a standard refractometer. The refractive index increment is expected to vary with the wavelength of the incident light (Machtle and Fischer, 1969), but because measurements were made with white light, the wavelength of measurement was difficult to define. For all of the solutions without glycerol, the molecular weight of BPTI determined from static light scattering at both 514 and 632.8 nm agrees with the known value of 6511 within ±10%, indicating this value is accurate and the wavelength dependence is small for BPTI. For the solutions that included glycerol, the molecular weights calculated used the literature *dn*/*dc* value gave a molecular weight that was significantly lower than the known value. This indicates that the value of the refractive index increment is lower in these solutions, as would be expected, because glycerol increases the solvent refractive index. Making the difference between the particle and solvent index smaller should reduce the value of *dn*/*dc*.

Even at the highest ionic strength investigated, there was no evidence from molecular weight determined from measured values of *dn*/*dc* that large aggregates existed in solution. This result is in agreement with dynamic light scattering results from Gallagher and Woodward (1989), who also showed BPTI to be a monomer in solutions between 0.1 and 0.5 M NaCl. Our results are in contrast with dynamic light-scattering results from Lafont et al. (1994), who found significant polydispersity in samples with 1 M NaCl or less, and dimers at higher ionic strengths even in very dilute solutions. Later experiments by Lafont et al. (1996) give evidence that BPTI exists as tetramers in high solvents with 1 to 2 M NaCl. In the static light-scattering results reported here, we found no evidence for this behavior.

Solubility was measured for BPTI by determining the concentration of protein in the liquid in equilibrium with a macroscopically observable solid. The method of achieving supersaturation was a membrane separation of the protein. Typically, the BPTI solutions were reconcentrated following static light scattering using both Centricon-3 and Centriprep-3 concentrators purchased from Amicon Inc., which have a molecular weight cutoff of 3000 M_W. Approximately 0.5 ml of pure solvent was allowed to pass through the membranes before use to remove glycerol and other additives that are shipped with the membrane. This method was used in order to reduce the amount of protein necessary for the study. The refractive index of the pure solvent remained unchanged when passing through the membrane, indicating that the components of the solvent did not partition in crossing the membrane. Because of the charge on the protein, however, a Donnan potential is expected across the membrane. Based on the method of Atkins (1990), at 1 M ionic strength, this effect would account for an ~2% increase in the ion concentration on the protein side of the membrane.

The concentrated solutions were allowed to equilibrate for a minimum of two weeks. If solids were observed in the samples, they were allowed to equilibrate for another week before solubility was determined. The concentration of protein in the mother liquor was determined by diluting a portion of the sample and measuring its absorbance at 280 nm. The solids in the protein solutions ranged from clear, well-formed crystals to white precipitates. This was assumed to be caused by the method of concentration, which could create areas of high concentration at the membrane surface as well as varying the supersaturation ratio from solution to solution.

RESULTS

At a pH of 4.9, the second virial coefficient of BPTI was measured at NaCl concentrations ranging from zero (buffer alone) to 1 M. As shown in Fig. 1, B_2 monotonically decreases with the particles being repulsive at low ionic strengths and attractive at higher salt concentrations. In this work we report second virial coefficients in units of volume rather than the more common form of $A_2 = B_2 N_A / M_w^2$. This is done to emphasize the statistical mechanical interpretation of the second virial coefficient as including a repulsive term due to excluded volume. Conversion from B_2 can be done by multiplying by 1.42×10^{22} to give A_2 in units of ml mol g^{-1}. If BPTI molecules interact as hard spheres (i.e., two BPTI molecules experience purely excluded volume interactions) with radii of 1.22 nm, BPTI would have a second virial coefficient of $B_{2hs} = 3.04 \times 10^{-26}$ m^3 ($A_{2hs} = 4.32 \times 10^{-4}$ ml mol g^{-1}). When $B_2/B_{2hs} = 1$, attractions and repulsions balance such that the molecules have thermodynamic properties of hard spheres. From the data in Fig. 1, this occurs at [NaCl] ~0.45 M. For lower ionic strengths, the change in B_2 with [NaCl] is suggestive of screening of electrostatic repulsions, whereas for a higher ionic strength, BPTI molecules experience an attraction.

Glycerol acts to increase the repulsions between BPTI molecules independent of the state of interaction in the absence of glycerol (Fig. 2). At 0.25 M NaCl in the absence of glycerol, BPTI molecules are repulsive. The strength of this repulsion is enhanced by the addition of glycerol. The difference between the values of B_2 in the absence and presence of 25 wt % glycerol is $\sim 1.65 \times 10^{-26}$ m^3, which is greater than the experimental uncertainties. The systematic increase in B_2 on addition of glycerol demonstrates an increased repulsion or a decreased attraction. At [NaCl] = 0.75 M and 1 M, addition of glycerol drives B_2 more positive again, indicating a reduction in strength of attraction or the increase in strength of repulsion. Note that the absolute change in B_2 on addition of glycerol is a weak function of [NaCl], suggesting that glycerol acts to change B_2 independently of other interactions.

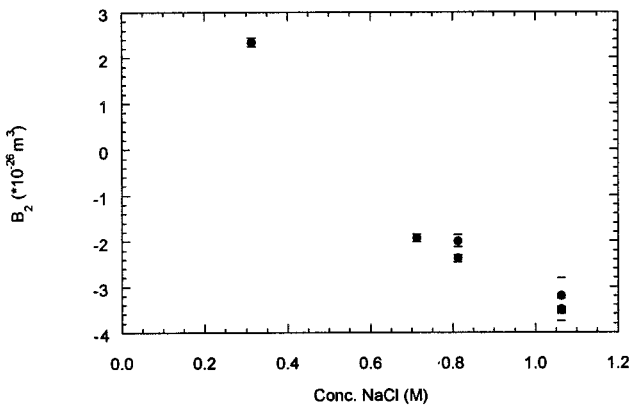

FIGURE 1 Second virial coefficient dependence of BPTI on added NaCl for pH 4.9 buffer. The circles indicate the data, and the bars represent the estimated uncertainty.

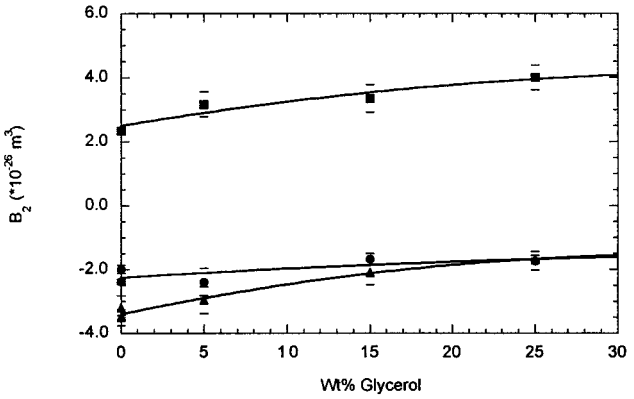

FIGURE 2 Second virial coefficient dependence on glycerol with 0.25 M NaCl (*squares*), 0.75 M NaCl (*circles*), and 1 M NaCl (*triangles*) in pH 4.9 acetate buffer. The lines are drawn to guide the eye.

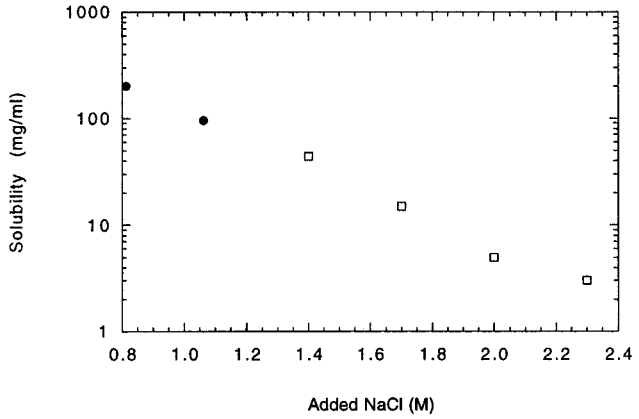

FIGURE 3 Solubility dependence of BPTI on added NaCl at pH 4.9. Circles represent data from this study, and squares represent data from Lafont et al., 1994.

The values for *dn*/*dc* used for the samples with 15 and 25 wt % glycerol were adjusted to ensure that in the limit of zero concentration, K*c*/*R* has the correct molecular weight. If the glycerol-free buffer value of *dn*/*dc* is used, the resulting molecular weights are lower than that of the monomer. The refractive index of the protein is greater than that of the solvent, as indicated by the positive value of *dn*/*dc*. With the addition of glycerol, the refractive index of the solvent increases appreciably, suggesting that the refractive index increment should decrease with [glycerol] as is observed with the values reported in Table 1.

BPTI solubility decreases with increasing ionic strength (Fig. 3). These results agree with the studies of Lafont et al. (1994), who also measured solubilities at pH 4.9 and show similar to the trends observed for silicotungstic acid (Zamora and Zukoski, 1996) and lysozyme (Howard et al., 1988; Rosenberger et al., 1993; Cacioppo and Pusey, 1991; Ewing et al., 1994; Rosenbaum and Zukoski, 1996). Salting out behavior is typical behavior for charged, globular macromolecules suspended in nonadsorbing electrolytes. With 1 M NaCl, glycerol increases the solubility of BPTI. As shown in Fig. 4, the largest effect occurs between zero and 5 wt % glycerol.

DISCUSSION

Detailed statistical mechanical calculations and simulations indicate that as B_2 grows more positive, a larger concentration of particles is required before an order/disorder phase transition will occur. As a reference point, consider that hard spheres crystallize at a volume fraction of 0.495 (Russel et al., 1989). Building on this result, as B_2/B_{2hs} approaches unity because of changes in [NaCl] or [glycerol], BPTI solubility is expected to approach ~660 mg/ml. This concentration lies outside the range where crystallographers typically work. Indeed, the cost of such experiments becomes prohibitive. By driving B_2/B_{2hs} to be less than one, the strength of attractive interactions are increased resulting in a reduction in solubility and an increase in the solubility gap (i.e., the difference in concentration in the ordered and disordered phases).

George and Wilson (1994) report that proteins are commonly crystallized from solutions resulting in slightly negative values of B_2. Care must be taken in interpreting this result, as the correlation of George and Wilson corresponds to initial conditions not those in which the crystal nucleated and grew. One of the most common techniques for crystallizing proteins is to hold temperature constant and allow solvent to evaporate. This increases protein concentration

TABLE 1 Refractive index increments values used for higher glycerol concentrations

Concentration of NaCl added (M)	Concentration of glycerol added (wt %)	*dn/dc* (ml/g)
0.25	15	0.178
0.25	25	0.176
0.75	15	0.180
0.75	25	0.172
1.0	15	0.182
1.0	25	0.170

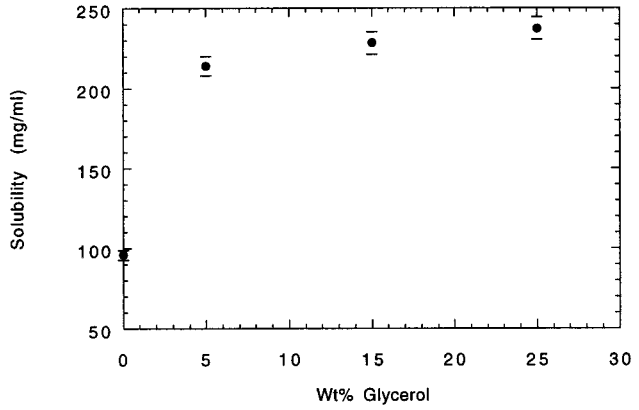

FIGURE 4 Solubility dependence of BPTI on added glycerol at 1 M NaCl in pH 4.9 buffer.

toward the solubility limit while also increasing the concentration of all nonvolatile solutes. If a hanging drop technique is used to crystallize BPTI and one starts at [NaCl] = 1 M, decreasing the drop volume by a factor of 2 will double protein concentration but will also decrease solubility by more than an order of magnitude. If glycerol is initially present, the solubility will not be decreased by the same amount, as [NaCl] and [glycerol] have opposite effects on solubility.

The subtle effects of solute concentration and type on protein interactions hinder finding solution conditions that generate high quality protein crystals and have led to efforts to develop systematic methods of characterizing protein interactions to reduce the empirical techniques in common usage. Our approach has been to develop generalized phase diagrams such that knowing the effects of chemical nature and concentration of solutes on protein interactions, one can rapidly design crystallization protocols.

Generalized phase diagrams are created by linking measures of the strength of protein interactions (relative to the system's thermal energy) to the protein concentration at phase boundaries. As a measure of the strength of the attraction, we have chosen B_2. In order to compare the link between B_2 and solubility for different proteins or for different solvent conditions, both the second virial coefficient and the solubility must be normalized. The second virial coefficients measured by static light scattering can be related to the interparticle pair potential, V(x), though statistical mechanics for spherical particles experiencing centrosymmetric interaction potentials from (McQuarrie, 1976)

$$B_2 = -2\pi\int_0^\infty x^2(e^{-V(x)/kT} - 1)dx \tag{3}$$

in which x is the distance between particle centers.

The integral expression in Eq. 3 is evaluated for center to center distances from ∞ to 0. To avoid particle overlap, the interaction potential is set to an arbitrarily large value for $x < 2a + \delta$, in which a is the hard core radius (1.22 nm) and δ is the distance of closest surface to surface approach. The continuum potentials typically used diverge at contact, and the introduction of δ eliminates this computational difficulty. For molecularly smooth surfaces, δ is expected to be on the order of 1 atomic diameter (0.1–0.2 nm). For proteins, which are not spheres and have complex surface topologies, a value of 0.1 nm represents a lower bound for the distance of closest approach for the equivalent spheres. Applying this condition, Eq. 3 becomes

$$B_2 = \left[\frac{2\pi}{3}(2a + \delta)^3\right] + \left[-2\pi\int_{2a+\delta}^\infty x^2(e^{-V(x)/kT} - 1)dx\right]. \tag{4}$$

The first term in Eq. 4 is the contribution from the hard core and remains constant regardless of the other values used in the pair potential. As a result, the hard sphere contribution, B_{2hs}, is defined as

$$B_{2hs} = \left[\frac{2\pi}{3}(2a + \delta)^3\right]. \tag{5}$$

To account for different hard core sizes, the second virial coefficients are normalized by the B_{2hs} value. Thus ($B_2/B_{2hs} - 1$) represents the contribution to the second virial coefficient due to particle interactions other than hard core excluded volume.

Solubilities are best compared in terms of volume occupied by the particles. As a result, solubilities are converted into the dimensionless number density, $\rho_{sat}(2a)^3$, which is directly proportional to the concentration of the fluid phase in equilibrium with a crystal, c_{sat},

$$\rho_{sat}(2a)^3 = \frac{c_{sat}N_A(2a)^3}{M_W}. \tag{6}$$

The solubilities and second virial coefficients for several proteins are given in Fig. 5. As discussed previously, the data for lysozyme (Rosenbaum, 1995; Rosenbaum et al., 1996; Rosenbaum and Zukoski, 1996; Gripon et al., 1997) and γ_{II}-crystallin (Fine et al., 1996) collapse onto a single curve. For changes in both ionic strength and glycerol concentration, the reduced second virial coefficients and solubilities for BPTI fall within the scatter of these results. In Fig. 5, a variety of solution conditions has been used, ranging from simple addition of electrolyte and temperature variation to using mixtures of D_2O and H_2O as cosolvents. That the changes in solubility produced by addition of glycerol fall on the correlation suggests that B_2/B_{2hs} is a robust indicator of solubility. Note that the presentation of

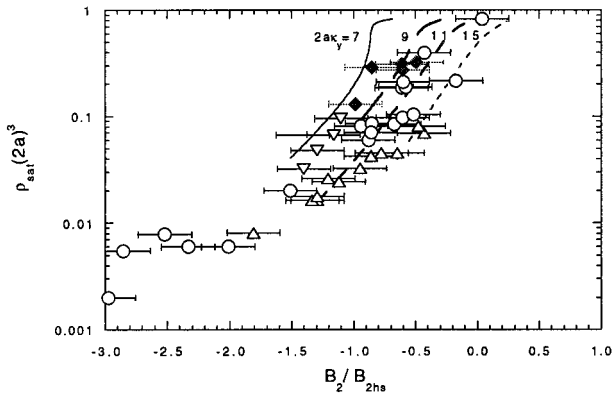

FIGURE 5 Normalized solubility ($\rho_{sat}(2a)^3$) and second virial coefficient (B_2/B_{2hs}) data for lysozyme, γ_{II}-crystallin, and BPTI. The data for BPTI, from this study, are represented by the filled diamonds. Data for lysozyme are represented by circles (Rosenbaum and Zukoski, 1996) and triangles (Gripon et al., 1997). Data for γ_{II}-crystallin are represented by inverted triangles (Fine et al., 1996). The lines are the solubility predictions of Hagen and Frenkel (1994) and Ramakrishnan (1998) for the Yukawa interaction potential with $2a\kappa_y$ ranging from 7 to 15, as indicated on the figure.

data in Fig. 5 is independent of model used to interpret B_2 or ρ_{sat}.

To develop insights on the origin of the correlation shown in Fig. 5 and thus to gain an appreciation of the limits of its application, we turn to theoretical descriptions of the links between particle interactions and phase behavior. Previous studies have compared solubilities with the phase diagram predicted for adhesive hard spheres (Rosenbaum et al., 1996). Here the strength of attraction $\tau = [1 - 4B_2/B_{2hs}]^{-1}$, thus making τ and B_2/B_{2hs} equivalent. As this potential has only two parameters (a and τ), a single phase diagram is predicted (Baxter, 1968). The adhesive hard sphere potential is one in which the particles have hard cores and interact with a square well attraction, which is infinitely narrow and infinitely deep.

For two parameter models, such as adhesive hard spheres or Lennard-Jones interactions, the phase behavior will be completely described in terms of two parameters: one characterizing the fraction of total system volume occupied by the particles ($(2a)^3\rho$) and a second characterizing the strength of interaction relative to the thermal energy in the system (typically taken as kT/ϵ_p, in which ϵ_p is the well depth, or τ in which for adhesive hard spheres is the stickiness parameter and plays the role of kT/ϵ_p) (Hansen and McDonald, 1976). As B_2 depends only on ϵ_p (or τ), a, and kT, a phase diagram drawn in terms of B_2/B_{2hs} versus $(2a)^3\rho$ is equivalent to the more common phase diagrams drawn in terms of kT/ϵ_p versus $(2a)^3\rho$. If the interaction potential contains a larger number of parameters, say both attractions and repulsions, or an attraction with a variable extent, a new phase diagram must be developed for each set of parameters.

Proteins clearly interact through a variety of mechanisms. These include van der Waals attractions, electrostatic repulsions, (noncentrosymmetric) dipole interactions, hydrophobic interactions, and hydrogen and ion bridge bonding mechanisms (Branden and Tooze, 1991). If each of these interactions could be broken out and varied independently of the others, an infinitude of phase diagrams could be predicted. However, B_2/B_{2hs} combines all these interactions into a single parameter representing the leading order term characterizing the nonidealities in suspension thermodynamics. As a result, B_2/B_{2hs} is often taken as a lumped parameter with which to characterize systems in which particles interact with complicated pair potentials and is found to greatly reduce the phase space that one must explore. In addition, B_2 has the advantage of being a directly measurable quantity, thus opening the possibility that phase behavior can be characterized without extensive but uncertain modeling efforts required to estimate protein interaction potentials. However, given the variety of pair potentials by which proteins interact, for a given value of B_2/B_{2hs} value, one might anticipate a wide variety of solubilities. The data in Fig. 5 indicate that a broad variety of proteins under a wide range of conditions have very similar phase behavior, thus raising the question of why solubility is so insensitive to details of the pair potential.

The adhesive hard sphere potential is of limited physical significance as true interactions have associated length scales and are not infinitely strong. One method of exploring why the phase diagrams are insensitive to details of the interaction potential is to consider the phase behavior predicted for a more complicated pair potential. A limited relaxation of the constraints of the adhesive hard sphere (AHS) potential can be made by allowing the particles to interact as spheres with a core radius a through a Yukawa potential:

$$V(x) = \begin{cases} \infty & x < 2a \\ -\epsilon_y \dfrac{\exp\left[2\kappa_y a\left(1 - \dfrac{x}{2a}\right)\right]}{\dfrac{x}{2a}} & x \geq 2a \end{cases} \qquad (7)$$

in which ϵ_y represents the strength of attraction, and κ_y^{-1} is the range of interaction. Hagen and Frenkel (1994) calculated the fluid phase (or solubility) boundary for a range of $a\kappa_y$ values showing that as $2a\kappa_y$ exceeds 7, the critical point for a fluid/fluid phase transition drops below the fluid crystal phase boundary. Their studies demonstrate that the only equilibrium phase transition seen for $2a\kappa_y > 7$ is that between a fluid and a crystal. For $2a\kappa_y > 7$, fluid/fluid transitions are predicted and experimentally observed to be metastable (Ries-Kautt and Ducruix, 1989; Muschol and Rosenberger, 1995; Taratuta et al., 1990; Rosenbaum, 1998). Assuming that for large values of $a\kappa_y$, the AHS condition is approached, Rosenbaum et al. (1996) converted the calculations of the phase diagram by Hagen and Frenkel for $2a\kappa_y = 9$ to the AHS phase diagram by equating second virial coefficients in the two systems.

Recognizing the need for a model independent method of displaying data we show in Fig. 5 predictions of the fluid/crystal phase boundary for several values of $2a\kappa_y$ (7, 9, 11, and 15) (Hagen and Frenkel, 1994; Ramakrishnan, 1998). As $2a\kappa_y$ is increased, the phase boundaries in B_2/B_{2hs} versus $(2a)^3\rho$ are weakly separated and, over a protein concentration range in which the calculations have been carried out, span the experimental data. Distinguishing different values of $2a\kappa_y$ from measurement of B_2 and solubilities lies outside the accuracy of extant data. Note however that $2a\kappa_y$ can be varied over a wide range producing a small change in B_2/B_{2hs} at a fixed solubility. Thus, whereas the proteins shown in Fig. 5 may interact with different potentials, the link between B_2/B_{2hs} and $\rho_{sat}(2a)^3$ is insensitive to these changes.

From the comparison in Fig. 5 of these three proteins under very different conditions, we conclude that when compared on an equal footing, these particles display very similar phase behavior. This result supports the hypothesis that the "crystallization slot" exists because broad classes of globular proteins interact with short-range attractions. Whereas the proteins may experience different pair potentials as electrolyte or solute concentration and type are altered because of the insensitivity of solubility to details of

the pair potential, the correlation between B_2/B_{2hs} and solubility will be robust as long as the extent of the attractions remains small.

The robustness of the B_2/solubility correlation is even more remarkable given the large dipolar interaction of BPTI molecules, which provides a first approximation of the attractions possible between proteins that have anisotropic charge distributions. The maximum interaction energy for two bare dipoles is given by (Israelachvili, 1992)

$$W = \frac{-2\mu^2}{4\pi\epsilon_0\epsilon(2a)^3}, \tag{8}$$

in which μ is the dipole moment and a is the particle radius. This interaction energy corresponds to the dipoles being oriented head to tail. At other orientations the dipole/dipole interaction will decrease. As the particles separate, the interactions are screened by the electrolyte. However, this anisotropic interaction potential scales on $\mu^2/(2a)^3$. Thus, small particles with modest dipole moments can have nonisotropic interaction energies that are quite large. For example, whereas μ is 280 Debye for BPTI, the strength of the dipole/dipole interaction is large given BPTI's small size. For BPTI, $W = 3.9$ kT, compared with 0.2 kT for lysozyme for this simple calculation. Recently, more detailed calculations of colloidal interactions including dipolar terms (Sader and Lenhoff, 1998; McClurg and Zukoski, 1998) indicate that dipole/dipole and charge/dipole interactions can be significant between proteins. The close similarity of the second virial coefficients and solubilities for BPTI and lysozyme suggests that these anisotropic interactions play a limited role in shifting the strength of interaction as measured by B_2 required to generate a given solubility.

Whereas the correlation in Fig. 5 provides a method for predicting solubility given second virial coefficient data, it provides little insight into the mechanism of change in B_2 with solvent conditions beyond their short-range nature. However, if we choose a form for $V(x)$, the data in Figs. 1–3 can be used to interpret the effects of solution conditions.

Before discussing the effect of glycerol on interactions of BPTI, the effects of [NaCl] must be treated first. Following a long tradition in discussing protein/protein interactions (Muschol and Rosenberger, 1995; Eberstein et al., 1994; Gallagher and Woodward, 1989), we treat BPTI as consisting of a hard, dielectric core with a uniform surface charge suspended in an electrolyte. Two BPTI molecules will thus feel at a minimum, van der Waals attractions and electrostatic repulsions and thus we use the well-known DLVO potential (Derjaguin and Landau, 1941; Verwey and Overbeek, 1948) for the interparticle potential outside of the overlap region ($r > 2a$). This approach attributes all repulsions to those due to the hard core and electrostatic repulsions and all attractions to the van der Waals forces. Despite these limitations, the DLVO potential captures the existence of an ionic strength dependent repulsion and a weak attraction, which characterizes protein interactions under crystallization conditions. Because the effect of glycerol on the bulk properties of the solvent other than the viscosity is minor (Miner and Dalton, 1953), our approach is to determine parameters for the DLVO potential that capture the behavior of BPTI in the absence of glycerol and then explore what possible mechanisms could be causing the increases in B_2 displayed in Fig. 2.

The DLVO potential is written:

$$V_{DLVO} = V_{VDW} + V_{ELEC} \tag{9}$$

in which V_{VDW} is the attractive interactions because of van der Waals forces, V_{ELEC} is the repulsive electrostatic interactions. The magnitude of the van der Waals force is determined by the Hamaker coefficient, A, and for two identical spheres has a form (Hamaker, 1937)

$$V_{VDW} = \begin{cases} \dfrac{-A}{6}\left(\dfrac{2r^2}{h^2+4ha} + \dfrac{2a^2}{(h+2a)^2} + \ln\left(\dfrac{h^2+4ha}{(h+2a)^2}\right)\right) & h > \delta \\ \infty & h \le \delta \end{cases} \tag{10}$$

in which h is the surface to surface separation, $x - 2a$.

For protein systems, the Hamaker coefficient has been measured to lie near 1 kT (Leckband et al., 1994). For globular proteins, A is typically estimated to lie between 1 and 2 kT (Nir, 1976). However, using the DLVO potential to fit of B_2 measurements, A is typically estimated as being substantially larger. For lysozyme, values from 4 to 9 kT (Muschol and Rosenberger, 1995; Eberstein et al., 1994) up to 55 kT for some models (Coen et al., 1995) have been used. For BPTI, a value of ~4.5 kT was used to fit dynamic light scattering data (Gallagher and Woodward, 1989). When using the DLVO potential to fit B_2, changes in δ by a fraction of a nanometer alter A by a factor of 2 indicating the extreme sensitivity of A to δ. Note however, that extracting A from light scattering data assigns all attractions to V_{VDW}. As a consequence, if hydrogen bonding or hydrophobic attractions are significant, they will act to artificially inflate the value of A.

The electrostatic portion of the interaction potential is represented by the Debye-Huckel approximation of the Poisson-Boltzman equation. In the case of low potentials, the interaction potential for two identical spheres is given by Russel et al. (1989)

$$V_{ELEC} = \frac{1}{4\pi\epsilon\epsilon_0}\left(\frac{z_p e}{1+\kappa a}\right)^2 \frac{a^2}{h+2a} e^{-\kappa h} \tag{11}$$

in which ϵ is the dielectric constant of the medium, ϵ_0 is the permitivity of free space, κ is the Debye-Huckel parameter, and z_p is the number of charges on the particle.

Using Eqs. 3 and 9–11, B_2 was evaluated for $z_p = +6.2$ (from the known amino acid sequence (Parkin et al., 1996) and pK_a values (Wuthrich and Wagner, 1979)), $A = 1$ kT, $a = 1.22$ nm, and $\delta = 0.1$ nm (dashed line in Fig. 6). Whereas these parameters capture the low ionic strength

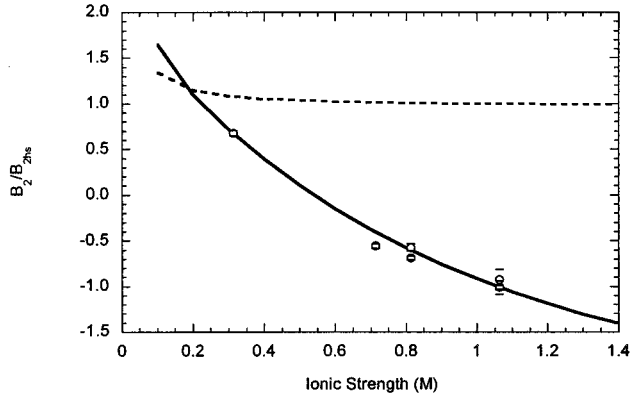

FIGURE 6 Prediction of second virial coefficients using the DLVO model. The dashed line represents the prediction based on a priori estimates of the parameters ($A = 1$ kT, $z_p = 6.2$, $r = 1.2235$ nm, $\delta = 0.1$ nm). The solid line represents the best fit prediction allowing the Hamaker coefficient and charge to vary (parameters ($A = 11.3$ kT, $z_p = 10.2$, $r = 1.2235$ nm, $\delta = 0.1$ nm).

behavior, these parameters overestimate B_2 (i.e., the attractions are larger than can be captured with the physically reasonable parameter values of d and A used here). The parameter that is least well established in the previous calculation is the cutoff distance, δ. By allowing the cutoff distance to shrink to 0.015 nm, predicted and measured virial coefficients can be brought into rough agreement (Farnum, 1997).

Because the literature values of the charge and Hamaker coefficient require an unphysical value of δ to fit B_2 over the entire ionic strength range, we choose to fix δ at 0.1 nm and allow z_p and A to be adjustable. Following Corti and Degiorgio (1981), at each ionic strength the values of z_p and A required for Eq. 4 to yield the measured value of B_2 were determined. The intersection of the curves occurs essentially at a single pair of z_p and A values yielding $z_p = +10.2$ and $A = 11.3$ kT. As shown in Fig. 6 (solid line), the predicted second virial coefficients calculated using these parameters fit the data very well.

The agreement of the model calculations and experimental results shown in Fig. 6 are consistent with previous studies (Muschol and Rosenberger, 1995; Rosenbaum and Zukoski, 1996), showing that B_2 can be modeled with the DLVO potential. The values for both the charge and Hamaker coefficient are substantially larger than expected. The value of A regressed from our data lies in the range of values used to fit second virial coefficient data gathered in other light scattering studies (Muschol and Rosenberger, 1995; Eberstein et al., 1994; Coen et al., 1995; Gallagher and Woodward, 1989), suggesting our data and fitting procedure are consistent with these previous studies but indicating that proteins tend to be more attractive than is expected on the basis of their dielectric properties alone. The large value of A required to fit B_2 data may be explained by recognizing that other interactions such as hydrogen bonding are not included in the DLVO potential such that in using Eq. 9, we are assigning all attractions to the van der Waals forces. However, if we choose to continue using the DLVO pair potential, possible explanations may be explored for the increased second virial coefficients with the addition of glycerol.

At the same electrolyte concentration, B_2 increases systematically with glycerol concentration. In the DLVO model, the addition of glycerol to the buffer most directly affects the dielectric constant. The change in adding 25 wt % glycerol, the highest amount used in this study, to water is slight, from 78.5 to 72.6 (Miner and Dalton, 1953). In the calculation of the second virial coefficient, the dielectric constant only appears directly in the equations that describe the electrostatic repulsion. If A and z_p are held constant at the values required to fit B_2 in the absence of glycerol, decreasing the dielectric constant increases B_2. However, this increase is small, ~3%, for ϵ changing from 78.5 to 72.6. To generate a repulsion large enough to explain the data would require a much larger change in ϵ, such as one that would apply to a 100% glycerol solution.

The dependence of the attractive force on the solvent does not appear directly in Eq. 10. However, the Hamaker coefficient, A, is a function of the solvent and particle properties, as shown in the following approximate equation (Israelachvili, 1992)

$$A = \frac{3}{4}kT\left(\frac{\epsilon_p - \epsilon_s}{\epsilon_p + \epsilon_s}\right)^2 + \frac{3h_p\nu_e(n_p^2 - n_s^2)^2}{16\sqrt{2}(n_p^2 + n_s^2)^{2/3}} \qquad (12)$$

in which ϵ_p is the dielectric constant of the particles, ϵ_s is the dielectric constant of the medium, h_p is Planc's constant, ν_e is the characteristic adsorption frequency, n_p is the refractive index of particles, and n_s is the refractive index of solvent.

With the addition of glycerol, the solvent dielectric constant and refractive index both are expected to be closer to the values for the protein core. The refractive index of the particle, n_p, can be estimated from the value of the refractive index, dn/dc. The difference between the particle refractive index in the solvent are related by

$$n_p - n_c = \frac{(dn/dc)M_W}{N_A(4/3\pi a^3)}. \qquad (13)$$

Using the value of dn/dc of Gallagher and Woodward (1989), in the absence of glycerol, $n_p = 1.6 \pm 0.2$. From Eq. 11 if we assume $u_e = 2 \times 10^{16}$ rad/sec (Nir, 1976), $A = 4.4$ kT, which is substantially less than the value of 11.3 kT required to fit the B_2 data. In the 25% glycerol buffer, the solvent refractive index is greater and dn/dc decreases to 0.17 ml/g. These changes in particle and solvent conditions result in decreasing A by ~1 to ~3.3 kT.

These estimates of A can be compared with those required to fit the experimental values of B_2 with fixed δ and a. If the DLVO model is applied to the 25% glycerol data, the Hamaker constant yielding the best fit to the B_2 data decreases, as expected, to a value of ~10.3 kT, whereas z_p increases to 11.6. The change in A when glycerol is added is comparable with that estimated from optical data. How-

ever, as the Hamaker coefficients predicted from optical data and those measured are much less than the values extracted from B_2 data, this agreement is most likely fortuitous.

A decrease in the strength of attraction or effective Hamaker coefficient could also be explained by a reduction in the other short-ranged forces between the protein molecules, such as the disruption of hydrogen bonds or hydrophobic contacts. The increase in charge might be explainable because of differential effects of ionization of surface groups caused by changes in ϵ. Confirmation of these changes requires further detailed electrokinetic studies.

An alternative interpretation may also be used to explain the decreased attraction or increased repulsion between BPTI molecules upon addition of glycerol. Glycerol is known to alter molecular volumes with typical effects being a reduction in the size of the core but an increase in the size of the hydration layers (Priev et al., 1996). Thus, glycerol could make the protein appear effectively larger or smaller. Because the mass of the protein is constant, its density should change with the $-1/3$ power of its radius. The value of the Hamaker coefficient depends on the square of the particle density (Israelachvili, 1992), so the variation with size should be

$$\frac{A_2}{A_1} \approx \left(\frac{\rho_2}{\rho_1}\right)^2 \approx \left(\frac{a_1}{a_2}\right)^6, \tag{14}$$

in which A_i, ρ_i, and a_i are the Hamaker coefficient, particle density, and particle radius in state i. Using this relationship makes the second virial coefficient a strong function of the size. Based on this analysis, increases by 0.05 nm can produce changes in B_2 sufficient to explain the observed changes on the addition of glycerol (Fig. 7).

Glycerol is also known to increase the size of the hydration layer at the particle surface (Timasheff and Arawaka, 1988). This change in the surface layer is best modeled as an increase in the cutoff distance used to truncate the van der Waals interactions near contact, δ. As shown in Fig. 8, a change in the cutoff distance of less than 0.01 nm would be large enough to account for the effect of glycerol on the measured values of B_2.

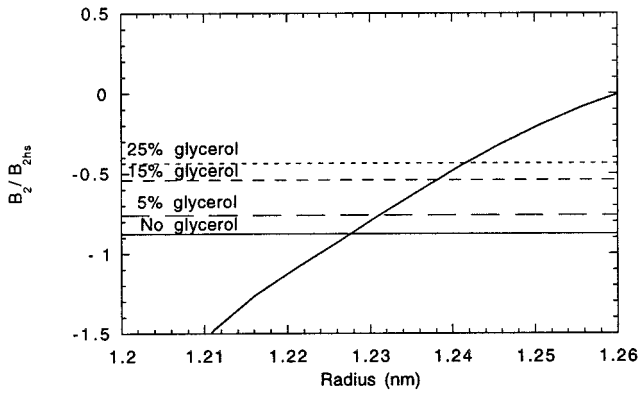

FIGURE 7 Prediction of the effect of size variation due to glycerol on the second virial coefficient at 1 M NaCl. The curve is the prediction. The solid line represents B_2 in the absence of glycerol. The dashed lines represent B_2 with increasing glycerol concentrations, 5, 15, and 25%, as indicated.

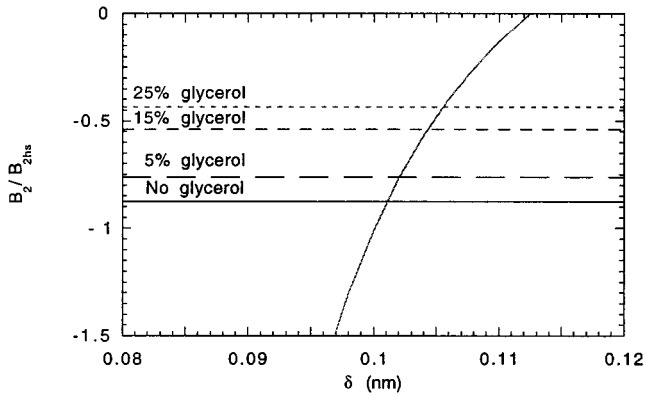

FIGURE 8 Prediction of the effect of increase hydration due to glycerol on the second virial coefficient at 1 M NaCl. The curve is the prediction. The solid line represents B_2 in the absence of glycerol. The dashed lines represent B_2 with increasing glycerol concentrations, 5, 15, and 25%, as indicated.

CONCLUSIONS

BPTI salts out of buffers at pH 4.9. However, the protein's solubility increases with the addition of glycerol. At the same time protein/protein interactions become more attractive as [NaCl] is increased but these interactions become more repulsive as [glycerol] is increased. Salting out can be understood in terms of an ionic strength dependent repulsion as anticipated for electrostatic repulsions in the presence of a short-range attraction. Attributing this attraction to van der Waals forces results in an unphysical Hamaker coefficient. The effects of glycerol can be understood in terms of altering protein size because of a small expansion of protein radius in the presence of glycerol or by the enhancement of a layer of solvent limiting the distance of closest approach. Given the known action of glycerol in stabilizing proteins against denaturation, we believe the best physical model is one incorporating a layer of structured water that is enhanced in the presence of glycerol. We note that if glycerol were treated like an osmolite, its addition would increase the strength of attraction because of depletion attractions (Russel et al., 1989; Gast et al., 1986). This effect was not observed at any ionic strength.

Whereas additional characterization techniques would be necessary to determine the origin of the attractions between BPTI molecules and the action of glycerol on these interactions, the central result of this work lies in the correlation between second virial coefficient and solubility. In this study we demonstrate that for an additional protein, the correlation between B_2/B_{2hs} and solubility remains robust when B_2 is altered by the addition of electrolyte and nonelectrolytes. This correlation can be understood in terms of statistical mechanical models demonstrating that globular

macromolecules experiencing short-range attractions will show phase behavior that is a weak function of the details of the pair potential. Indeed, the presence of considerable dipolar interactions between BPTI molecules does not appear to detract from this correlation.

Whereas our investigation provides further support for the observation of George and Wilson (1994), we also continue the generalization of their approach by indicating that the "crystallization slot" can be quite extensive and results from fundamental nature of the links between nonidealities in solution thermodynamic behavior and the solubility limit. Details of the interactions will vary from protein to protein and cosolute to cosolute. However, the narrow band of B_2/B_{2hs} resulting in similar solubilities suggests that under conditions in which the solvent contains molecules substantially smaller than the protein, the attractive well is narrow with respect to the protein core diameter resulting in a very limited and closely related set or phase boundaries. However, if more complex crystallizing conditions are used where the interaction potential is no longer monotonically attractive (such as at lower ionic strengths or in the presence of polymers) this correlation between B_2/B_{2hs} and solubility may fail. However, the large set of conditions and proteins investigated in Fig. 5 indicates that there are broad ranges of proteins and crystallizing conditions in which measurement of B_2 offers a rapid, nondestructive screening method for determination of good crystallizing conditions.

The authors thank S. Ramakrishnan for his calculations of phase boundaries. This work was supported by NASA Grant NAG8–976.

REFERENCES

Amir, D., S. Krausz, and E. Hass. 1992. Detection of local structures in reduced unfolded bovine pancreatic trypsin inhibitor. *Proteins Struct. Funct. Genet.* 13:162–173.

Atkins, P. W. 1990. Physical Chemistry, 4th ed. W. H. Freeman and Company, New York.

Baxter, R. J. 1968. Percus-Yevick equation for hard spheres with surface attraction. *J. Chem. Phys.* 49:2770–2774.

Branden, C., and J. Tooze. 1991. Introduction to Protein Structure. Garland Publishing, New York.

Cacioppo, E., and M. L. Pusey. 1991. The solubility of the tetragonal form of hen egg white lysozyme from pH 4.0 to 5.4. *J. Cryst. Growth.* 144:286–292.

Coen, C. J., H. W. Blanch, and J. M. Prausnitz. 1995. Salting out of aqueous proteins: phase equilibria and intermolecular potentials. *AIChE J.* 41:996–1004.

Corti, M., and V. Degiorgio. 1981. Quasi-elastic light scattering study of intermicellar interactions in aqueous sodium dodecyl sulfate solutions. *J. Phys. Chem.* 85:711–717.

Coumou, D. L. 1960. Apparatus for the measurement of light scattering in liquids: measurement of the Raleigh factor of benzene and of some other pure liquids. *J. Coll. Sci.* 15:408–417.

Coumou, D. L., and E. L. Mackor. 1964. Isotropic light scattering in binary liquid mixtures. *Trans. Faraday Soc.* 60:1726–1735.

Coumou, D. L., E. L. Mackor, and J. Hijmans. 1964. Isotropic light-scattering pure liquids. *Trans. Faraday Soc.* 60:1539–1547.

Creighton, T. E. 1974. Renaturation of the reduced pancreatic trypsin inhibitor. *J. Mol. Biol.* 87:563–577.

Deisenhofer, J., and W. Steigemann. 1975. Crystallographic refinement of the structure of bovine pancreatic trypsin inhibitor at 1.5 Å resolution. *Acta Cryst.* B31:238–250.

Derjaguin, B. V., and L. D. Landau. 1941. Theory of stability of strongly charged lyophobic sols and the adhesion of strongly charged particles in solutions of electrolytes. *Acta Physicochimica URSS* 14:633–662.

Drenth, J. 1994. Principles of Protein X-Ray Crystallography. Springer-Verlag, New York.

Eberstein, W., Y. Georgalis, and W. Saenger. 1994. Molecular interactions in crystallizing lysozyme solutions by photon correlation spectroscopy. *J. Cryst. Growth.* 143:71–78.

Ewing, F., E. Forsythe, and M. Pusey. 1994. Orthorhombic lysozyme solubility. *Acta Cryst.* D50:424–428.

Farnum, M. 1997. BPTI solubility and interactions in the presence of glycerol. Master's Thesis, University of Illinois.

Fine, B. M., A. Lomakin, O. O. Ogun, and G. B. Benedek. 1996. Static structure factor and collective diffusion of globular proteins in concentrated aqueous solution. *J. Chem. Phys.* 104:326–335.

Gallagher, W. H., and C. K. Woodward. 1989. The concentration dependence of the diffusion coefficient for bovine pancreatic trypsin inhibitor: a dynamic light scattering study of a small protein. *Biopolymers.* 28: 2001–2024.

Gast, A. P., W. B. Russel, and C. K. Hall. 1986. An experimental study of phase transitions in the polystyrene latex and hydroxyethylcullulose system. *J. Coll. Int. Sci.* 109:161–171.

Gekko, K., and S. N. Timasheff. 1981. thermodynamics and kinetic examination of protein stabilization by glycerol. *Biochemistry.* 20: 4677–4686.

George, A., Y. Chang, B. Guo, A. Arabshahi, Z. Cai, and W. Wilson. 1997. Second virial coefficient as predictor in protein crystal growth. *Methods Enzymol.* 276:100–110.

George, A., and W. Wilson. 1994. Predicting protein crystallization from a dilute solution property. *Acta Cryst.* D50:361–365.

Gripon, C., L. Legrand, I. Rosenman, O. Vidal, M. C. Robert, and F. Boue. 1997. Lysozyme-lysozyme interactions in under- and super-saturated solutions: a simple relation between the second virial coefficients in H_2O and D_2O. *J. Cryst. Growth.* 178:575–584.

Hagen, M. H. J., and D. Frenkel. 1994. Determination of phase diagrams for the hard-core attractive Yukawa system. *J. Phys. Chem.* 98: 10358–10367.

Hamaker, H. C. 1937. London-van der Waals attraction between spherical particles. *Physica.* 4:1058–1072.

Hansen, J. P., and I. R. McDonald. 1976. Theory of Simple Liquids. Academic Press, New York.

Howard, S. B., P. J. Twigg, J. K. Baird, and E. J. Meehan. 1988. The solubility of hen egg-white lysozyme. *J. Cryst. Growth.* 129:94–104.

Israelachvili, J. 1992. Intermolecular and Surface Forces, 2nd ed. Academic Press, London.

Kassell, B. 1970. Bovine trypsin-kallikrein inhibitor (kunitz inhibitor, basic pancreatic trypsin inhibitor, polyvalent inhibitor from bovine organs). *Methods Enzymol.* 19:884–852.

Kaye, W., and J. B. McDaniel. 1974. Low-angle laser light scattering: rayleigh factors and depolarization ratios. *Appl. Optics.* 13:1934–1937.

Kerker, M. 1969. The Scattering of Light and Other Electromagnetic Radiation. Academic Press, New York.

Lafont, S., S. Veesler, J. P. Astier, and R. Boistelle. 1994. Solubility and prenucleation of aprotinin (BPTI) molecules in sodium chloride solutions. *J. Cryst. Growth.* 143:249–255.

Lafont, S., S. Veesler, J. P. Astier, and R. Boistelle. 1996. Prenucleation and crystallization of proteins: application to BPTI solutions. *Chem. Eng. Res. Design.* 74:839–843.

Lafont, S., S. Veesler, J. P. Astier, and R. Boistelle. 1997. Comparison of solubilities and molecular interactions of BPTI molecules giving different polymorphs. *J. Cryst. Growth.* 173:132–140.

Lakowicz, J. R., G. Laczkko, and I. Gryczynski. 1987. Picosecond resolution of tyrosine fluorescence and anisotropy decays by a 2-GHz frequency-domain fluorometry. *Biochemistry.* 26:82–90.

Leckband, D. E., F. J. Schmitt, J. N. Israelachvili, and W. Knoll. 1994. Direct force measurements of specific and nonspecific protein interactions. *Biochemistry.* 33:4611–4624.

Machtle, W., and H. Fischer. 1969. Zum spezifixshen brechungsinkremnt von homo- und copolymerlosungen. *Angewandie Makromolekulare Chemie.* 7:147–180.

Makhatadze, G. I., K. Kim, C. Woodward, and P. L. Privalov. 1993. Thermodynamics of BPTI folding. *Protein Sci.* 2:2028–2036.

McClurg, R., and C. F. Zukoski. 1998. The electrostatic interaction of rigid, globular proteins with arbitrary change distributions. *J. Colloid Interface Sci.* In press.

McPherson, A. 1982. Preparation and Analysis of Protein Crystals. Wiley, New York.

McPherson, A. 1990. Current approaches to macromolecular crystallization. *Eur. J. Biochem.* 189:1–23.

McQuarrie, D. 1976. Statistical Mechanics. HarperCollins, New York.

McRee, D. E. 1993. Practical Protein Crystallography. Academic Press, New York.

Miner, C. S., and N. N. Dalton. 1953. Glycerol. Reinhold Publishing, New York.

Muschol, M., and F. Rosenberger. 1995. Interactions in undersaturated and supersaturated lysozyme solutions: static and dynamic light scattering results. *J. Chem. Phys.* 103:10424–10432.

Muschol, M., and F. Rosenberger. 1995. Liquid-liquid phase separation in supersaturated lysozyme solutions and associated precipitate formation/crystallization. *J. Chem. Phys.* 107:1952–1963.

Nir, S. 1976. van der Waals interactions between surfaces of biological interest. *Prog. Surf. Sci.* 8:1–58.

Parkin, S., B. Rupp, and H. Hope. 1996. Structure of bovine pancreatic trypsin inhibitor at 125K: definitions of carboxyl-terminal residues Gly57 and Ala58. *Acta Cryst.* D52:18–29.

Priev, A., A. Almagor, S. Yedgar, and B. Gavish. 1996. Glycerol decreases the volume and compressibility of protein interior. *Biochemistry.* 35:2061–2066.

Ramakrishnan, S. 1998. Thermodynamics and Phase Behavior of Nanoparticles. Master's Thesis, University of Illinois.

Ries-Kautt, M. M., and A. F. Ducruix. 1989. Relative effectiveness of various ions on the solubility and crystal growth of lysozyme. *J. Biol. Chem.* 264:745–748.

Rosenbaum, D. F. 1995. Protein Phase Boundary Predictions from Dilute Solution Properties. Master's Thesis, University of Illinois.

Rosenbaum, D. F. 1998. An Investigation of Protein Interactions and the Relationship to Phase Behavior. Ph. D. Thesis, University of Illinois.

Rosenbaum, D. F., P. C. Zamora, and C. F. Zukoski. 1996. Phase behavior of small attractive colloidal particles. *Phys. Rev. Lett.* 76:150–153.

Rosenbaum, D., and C. F. Zukoski. 1996. Protein interactions and crystallization. *J. Cryst. Growth.* 169:752–758.

Rosenberger, F., S. B. Howard, J. W. Sowers, and T. A. Nyce. 1993. Temperature dependence of protein solubility - determination and application to crystallization in x-ray capillaries. *J. Cryst. Growth.* 129:1–12.

Russel, W. B., D. A. Saville, and W. R. Schowalter. 1989. Colloidal Dispersions. Cambridge University Press, Cambridge.

Sader, J. E., and A. M. Lenhoff. 1998. Electrical double-layer interaction between heterogenoeously charged colloidal particles: a superposition formulation. *J. Coll. Int. Sci.* 201:233–243.

Scholtan, W., and S. Y. Lie. 1966. Molekulargewichtsbestimmung des kallikrein-inaktivators mittels der ultracentrifuge. *Die Makromolekulare Chemie.* 98:204–234.

Sousa, R. 1995. Use of glycerol and other protein structure stabilizing agents in protein crystallization. *Acta Cryst.* D51:271–277.

Taratuta, V. G., A. Holschbach, G. M. Thurston, D. Blankschtein, and G. B. Benedek. 1990. Liquid-liquid phase separation of aqueous lysozyme solutions: effects of pH and salt identity. *J. Phys. Chem.* 94:2140–2144.

Timasheff, S. N., and T. Arakawa. 1988. Mechanism of protein precipitation and stabilization by co-solvents. *J. Cryst. Growth.* 90:39–46.

Verwey, E. J. W., and J. Th. G. Overbeek. 1948. Theory of the Stability of Lyophobic Colloids. Elsevier, Amsterdam.

Wills, P. R., and Y. Georgalis. 1981. Concentration dependence of the diffusion coefficient of a dimerizing protein: bovine pancreatic trypsin inhibitor. *J. Chem. Phys.* 85:3978–3984.

Wuthrich, K., and G. Wagner. 1979. Nuclear magnetic resonance of labile protons in the basic pancreatic trypsin inhibitor. *J. Mol. Biol.* 130:1–18.

Zamora, P. C., and C. F. Zukoski. 1996. Interactions and phase behavior of nanosized particles. *Langmuir.* 12:3541–3547.